Very High-Speed Light-Source Module up to 40 Gb/s Containing an MQW Electroabsorption Modulator Integrated with a DFB Laser

Hiroaki Takeuchi, Ken Tsuzuki, Kenji Sato, *Member, IEEE,* Mitsuo Yamamoto, Yoshio Itaya, Akihide Sano, Mikio Yoneyama, and Taiichi Otsuji

Abstract—A very high-speed integrated light source up to 40 Gb/s has been developed. The integrated light source consists of an multiple-quantum-well (MQW) electroabsorption (EA) modulator and a distributed-feedback (DFB) laser. After optimizing the structure of the integrated modulator, the device is packaged in a compact module with a single-mode fiber (SMF). While the DFB laser is injected with a constant current, the integrated MQW electroabsorption modulator is driven with a 40-Gb/s electrical NRZ signal. A clearly-open eye diagram is observed in the modulated light from the modulator. Further, a receiver sensitivity of −27.2 dBm at 10^{-9} is experimentally confirmed in bit-error-rate (BER) performance. Highly resolved optical short pulse is also generated at a repetition rate of 40 GHz using the new light-source module.

Index Terms— Distributed-feedback laser, electroabsorption modulator, multiquantum well.

I. Introduction

THE ELECTROABSORPTION (EA) modulator is very promising device for application to future optical transmission systems such as high-speed or wavelength-multiplexing systems. It offers many advantages, for example, low-chirp or blue-chirp characteristics [1]–[3], small size, and easy integration with lasers and other waveguide devices. In particular, the EA modulators with a multiple-quantum-well (MQW) as an absorption layer have been very widely studied. These have so far achieved an ultrahigh-speed modulation over 40 GHz [4]–[7], a low driving voltage [8], and a high modulation efficiency [9]. For application to light sources in optical transmission systems, the EA modulator should be integrated with a single-mode oscillating laser to fully utilize its compactness. Consequently, many studies have been reported on EA modulators integrated with a distributed-feedback (DFB) laser.

The modulation speed of an MQW EA modulator is limited by its electrical capacitance. As a result, a shorter modulator length is preferable for this purpose. The largest 3-dB bandwidth, as far as we know, of an EA modulator integrated with

a DFB laser is 36 GHz [10]. The highest bit rate reported so far in transmission experiments has been 20 Gb/s [11], [12]. Transmission at much higher bit rates has never been carried out due to the relatively poor bandwidth of the modulator and difficulties with generating a driving electrical signal. MQW EA modulators integrated with DFB lasers have another important application of the light source in generating optical short-pulse trains. Transform-limited sech or Gaussian optical pulses can easily be generated by applying sinusoidal reverse voltage. The highest repetition rate, as far as we know, is 30 GHz by this simple generating method [13].

In this paper, we describe a very high-speed light source module containing an MQW EA modulator integrated with a DFB laser. This light source module exhibited a successful 40-Gb/s nonreturn-to-zero (NRZ) operation and highly resolved optical pulse trains at a repetition rate of 40 GHz. We introduced butt-joint technology to integrate the EA modulator and the DFB laser, which produced an efficient coupling of 95% and made it easy to optimize the structure of the integrated EA modulator. A larger well number of 14 in the absorption MQW and a shorter length of 90 μm in the EA modulator achieved a 3-dB bandwidth over 30 GHz. After the device was packaged in a compact module with a single mode fiber, we successfully achieved 40-Gb/s NRZ operation, for the first time, by using the MQW EA modulator integrated with the DFB laser. While the DFB laser was injected with a constant current, the integrated MQW electroabsorption modulator was driven with a 40-Gb/s electrical NRZ signal. A clearly-open eye diagram was observed in the modulated light from the modulator. Further, a receiver sensitivity of −27.2 dBm at 10^{-9} was experimentally confirmed in bit-error-rate (BER) performance. We also obtained optical short pulse trains at a repetition rate of 40 GHz using the new light-source module, which is the highest rate, as far as we know, using a simple method of applying sinusoidal reverse voltage.

II. Device Structure and Fabrication

The structure of the integrated light source is schematically shown in Fig. 1. This integrated device consists of an EA modulator and a DFB laser. We used butt-joint technology to integrated the EA modulator and the DFB laser on an InP chip. Several integration technologies have been used in the previous papers, that is, stacked-layer technology [11], butt-joint technology [14], selective-area-growth technology
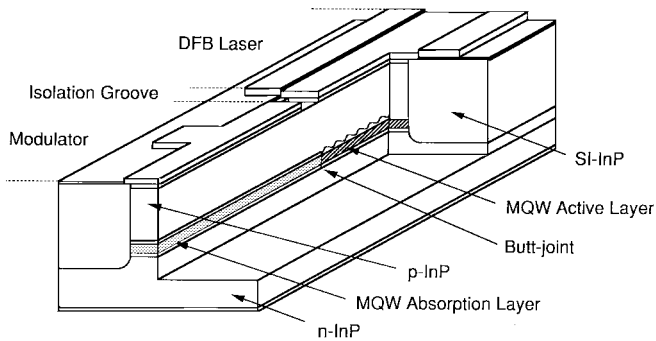
Fig. 1.   Schematic view of the MQW electroabsorption modulator integrated with a DFB laser.

MQW absorption layer of the modulator

The well is compressively strained by 0.5%.
The barrier is tensilely strained for stress compensation.

Guide:*InGaAsP(1.10 μm)*	80 nm or 50 nm
Well: *InGaAsP*	9.7 nm
Barrier:*InGaAsP(1.10 μm)*	5.0 nm
	8 & 14 Wells
Barrier:*InGaAsP(1.10 μm)*	5.0 nm
Well: *InGaAsP*	9.7 nm
Guide:*InGaAsP(1.10 μm)*	80 nm

(a)

MQW active layer of the DFB laser

The well is compressively strained.

Guide:*InGaAsP(1.25 μm)*	70 nm
Well: *InGaAsP*	6.7 nm
Barrier:*InGaAsP(1.25 μm)*	15.1 nm
Barrier:*InGaAsP(1.25 μm)*	6.7 nm
Well: *InGaAsP*	15.1 nm
Guide:*InGaAsP(1.25 μm)*	70 nm

(b)

Fig. 2.   The MQW structures of the EA modulator and the DFB laser.

[15]–[19], and identical layer technology [12]. Among them, the butt-joint technology is the most attractive since it allows us to optimize the structure of the EA modulator and the DFB laser independently.
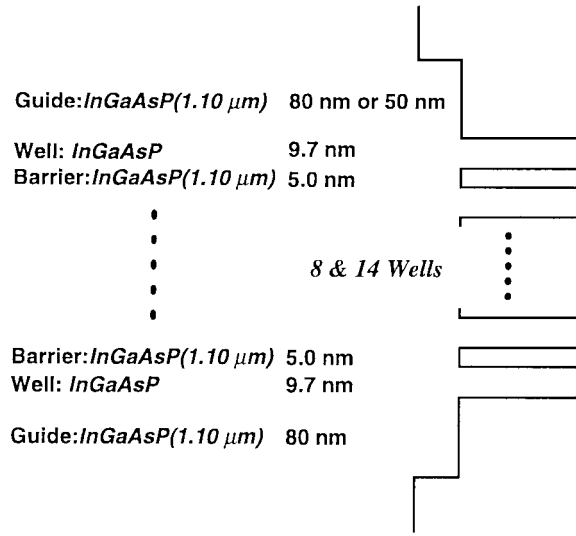
In the fabrication process, six pairs of strained InGaAsP multiple MQW's were grown on an n-type (100) InP substrate as the active layer of a DFB laser by low-pressure metalorganic vapor phase epitaxy (MOVPE). The wells were 6.7-nm-thick InGaAsP with compressive strain and the barriers were 15.1-nm-thick InGaAsP with a photoluminescence wavelength of 1.25 μm. The MQW active layer was etched off down to the substrate except in the DFB laser region. Then, an additional InGaAsP MQW, with a well of 9.7-nm-thick InGaAsP and a barrier of 5-nm-thick InGaAsP, was selectively grown as an absorption layer of the modulator. The well was compressively strained by 0.5% and the barrier was tensilely strained to compensate for the strain of the MQW. The MQW of the EA modulator and the DFB laser are illustrated in Fig. 2. A butt-joint configuration was thus formed between the the DFB laser and the electroabsorption modulator. After a corrugation grating was formed in the DFB laser, a p-type InP cladding layer and p-type contact layer were successively grown. The epitaxial layers including the MQW active and the MQW absorbing layers were formed in a 2-μm-wide high-mesa ridge structure by a dry etching technique. The modulator and the DFB laser were buried in Fe-doped InP to reduce electric capacitance and to form the surface plane. An Fe-doped InP buried structure has the advantage of yielding high optical power due to low thermal resistance and is expected to be very reliable in long-term operation [20]. An isolation groove was then formed between the DFB laser and the modulator, followed by electrode formation. The devices were cleaved into a chip, in which the length of the modulator and the DFB laser were from 90 to 250 μm and 450 μm, respectively. The facets were coated with an AR film for the modulator and with a high-reflection film for the DFB laser. Finally, the integrated light source was packaged into a compact module with a single-mode fiber (SMF) pigtail for measurement.

III. DEVICE DESIGN FOR HIGH-SPEED OPERATION

The operation speed of the EA modulator is limited by its capacitance. Shorter modulator length and smaller electric capacitance are desirable for achieving high-speed operation of the EA modulator. However, reduction 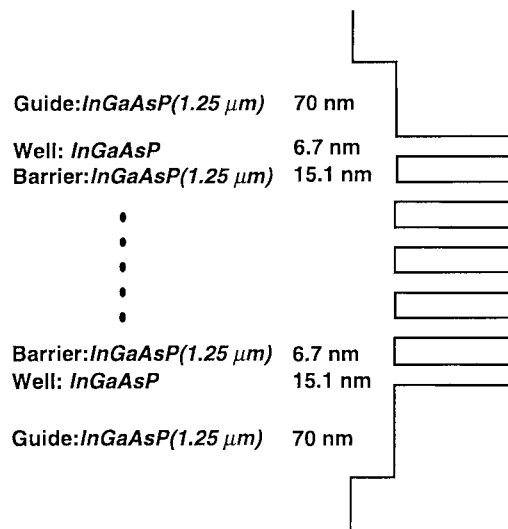of the modulator length yields a smaller extinction ratio in attenuation characteristics. This is quite problematic in practical use. We expected to overcome the problem by equipping the modulator with a larger number of wells in the MQW of the EA modulator. Before
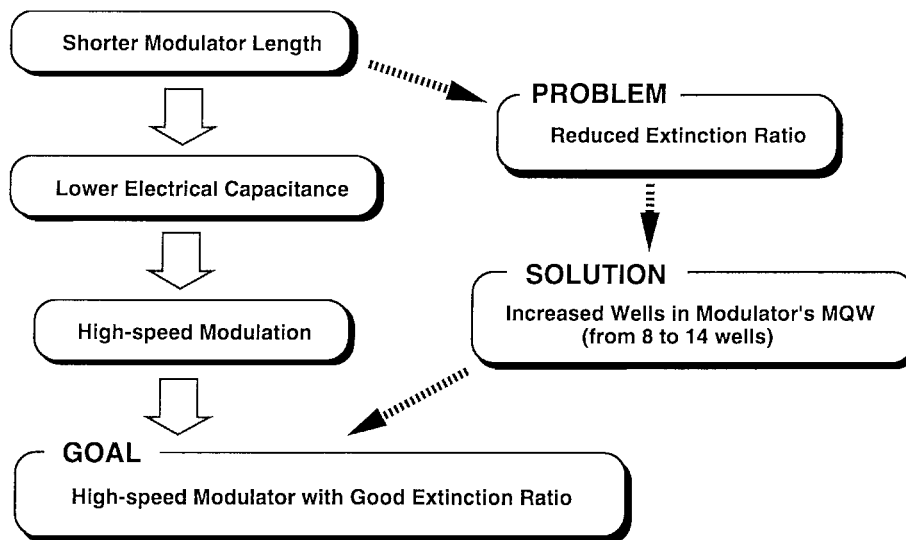
Fig. 3. The procedure for the high-speed EA modulator.

this work we used eight wells, however here, we introduced an MQW absorption layer with 14 wells in the integrated EA modulator to build a high-speed modulator with a good extiction ratio. The above-mentioned procedure to develop the high-speed integrated EA modulator is summarized in Fig. 3. This optimization was possible by introducing the butt-joint technology, as previously mentioned.

IV. EXPERIMENTAL RESULTS

A. Static Performance

The coupling efficiency at the butt-joint between the DFB laser and the EA modulator with a 14-MQW well was measured. This was determined from the measurement of the output power from the integrated EA modulator as a function of the current to the DFB laser (the I–L measurement). In the I–L measurement, all the output power from the facet was observed using a large detector. We measured the ratio of the output power when deeply reverse-biased to the integrated modulator against that when open-circuited. Then, we estimated the coupling efficiency by subtracting the measured ratio from 1. This estimation included the following two assumptions; the extinction ratio was enough large when deeply reverse-biased and the propagation loss of the integrated EA modulator under when open-circuited was negligible. This method was quite simple and gave us a reliable value especially when the EA modulator had a large extinction ratio. The estimated coupling efficiency is shown in Fig. 4. We measured sixteen devices selected at random. The efficiency was over 90% for all samples except one. The average efficiency was about 95%. We also measured the coupling efficiency for the integrated light source with 8 wells in the absorption MQW, which was almost the same as that for 14 wells.

The propagation loss of the integrated EA modulator was also measured. We increased the MQW well number of the absorption layer up to 14 to obtain high-speed operation. Because the larger well number might increase loss of the integrated EA modulator, we measured this using two modulators with 8 and
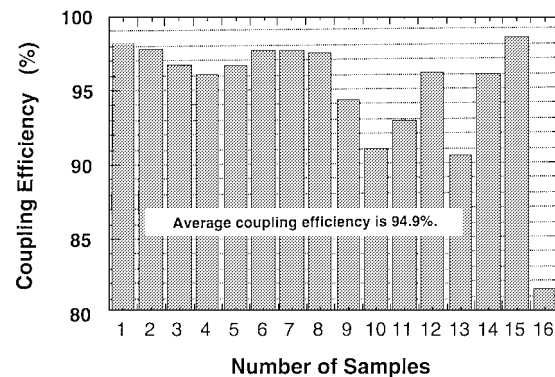

Fig. 4. The measured coupling efficiency at the butt-joint.

14 wells and a length of 225 μm. During the measurement, the modulators were short-circuited. The total loss and the loss per unit length of the modulator when short-circuited are plotted in Fig. 5. Two well numbers, 8 and 14, are shown for comparison. In the MQW EA modulator, the extinction characteristics comes from the quantum confined stark effect (QCSE) by applying reverse voltage. The exciton-peak wavelength moves toward a longer wavelength under reverse voltage and the fed light into the integrated EA modulator from the DFB laser is absorbed. Thus, the loss and the extinction characteristics heavily depend on the wavelength difference between the exciton-peak wavelength and the oscillating wavelength of the DFB laser, which we call the detuning wavelength. In the actual measurements, we defined the detuning wavelength as the difference between the photoluminescence (PL) wavelength of the MQW of the modulator and the DFB lasing wavelength. Then, we plotted the loss of the integrated EA modulator as a function of the detuning wavelength in Fig. 5. The losses in the 8 and 14 wells exhibit no difference at larger detuning wavelengths of more than 60 nm. They show a steep increase when the detuning wavelength decreases. The smaller detuning wavelength causes large undesirable loss and the larger detuning wavelength produces large driving voltage. Consequently, we selected a detuning wavelength from 50 to
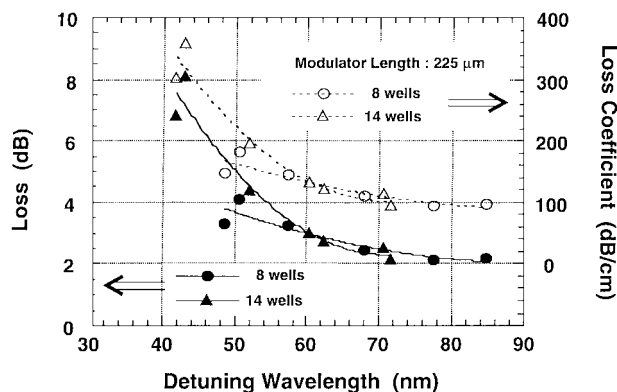
Fig. 5. The total loss and the loss per unit length of the integrated EA modulator.

Fig. 7. Dependence of the extinction ratio on the MQW well number of the EA modulator.
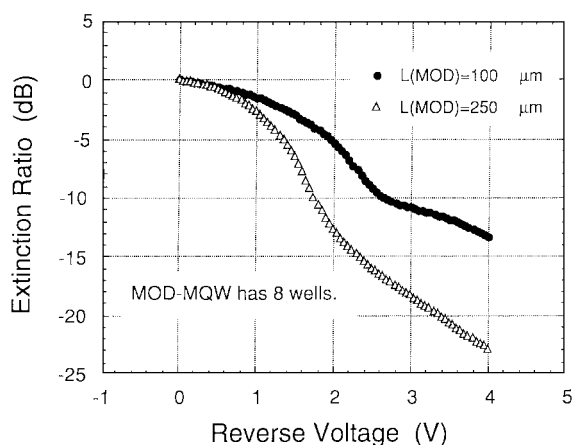

Fig. 6. Dependence of the extinction ratio on the EA modulator length.

60 nm for our integrated light source. Fortunately, the loss did not exhibit large increase in this range when we used the 14 wells shown in Fig. 5.

Here, the extinction ratio dependence on the modulator length is plotted in Fig. 6 as a function of the reverse voltage. The extinction characteristics between two different modulator lengths of 100 and 250 μm were compared. In these measurements, the well number of the modulator was equal to 8 and the detuning wavelength was about 56 nm for both samples. Although the shorter modulator 100 μm produces higher-speed operation, the extinction ratio is not enough large to meet system requirements. With eight wells, the obtained extinction ratio was only 13 dB at a reverse voltage of 4 V. A simple and effective method to overcome the problem is to increase the number of MQW wells in the EA modulator.

The dependence of the extinction characteristics on the number of MQW wells in the EA modulator is shown in Fig. 7. The length of the integrated modulator was set at 100 μm for the two samples (8 and 14 wells). The detuning wavelengths were in a range from 56 to 59 nm. Increasing the well number up to 14 resulted in a very clear improvement in the extinction characteristics. The optical confinement factor of the absorption MQW layer increases along with the number of MQW wells as shown in Fig. 8. Here, the absorption MQW consists of a well of 9.7-nm-thick InGaAsP and a
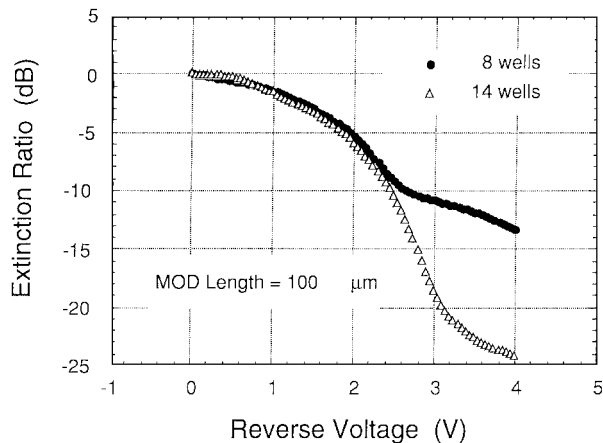
barrier of 5-nm-thick InGaAsP as previously described. The confinement factors were 0.17 and 0.36 for well numbers of 8 and 14. The absorption in the MQW was linearly proportional to the confinement factor. Consequently, the difference in the confinement factor was one reason the extinction ratio improved because of the larger MQW well number of 14. However, in Fig. 7, the extinction ratios under reverse voltages of less than 2.3 V were almost the same. To analyze these discrepancies, we calculated the electrical field distribution in the absorption MQW as a function of the applied reverse voltage. The layered structure used in the calculation is shown in Fig. 2. The carrier concentrations were assumed to be 5×10^{17}, 1×10^{16}, and 1×10^{18} cm^{-3} for the p-InP, the undoped layers including the MQW, and the n-InP, respectively. The obtained electrical field distribution is plotted in Fig. 9. The electrical field intensity in the MQW with 14 wells is smaller than that of the one with 8 wells at fixed reverse voltage. Also, the electrical field in the MQW decreases toward the direction of the n-InP due to the residual carrier concentration of the undoped layers. These decreasing characteristics are apparent especially in the 14 thicker wells. Consequently, the region with weak electrical field in the 14-well MQW is wider than that in the 8-well MQW. The absorption based on the QCSE is a function of the electrical field. The dependence on the electrical field is very complicated because of the broadening of the exciton peak under reverse voltage [21]. However, we believe that the different electrical field distributions for the 8 and 14 wells can be explained by the characteristics in Fig. 7.

Based on these results, we prepared an integrated light source containing a modulator with 14 wells in the MQW and with a detuning wavelength of about 60 nm for the 40-Gb/s operation experiments. The integrated light source chip had a 450-μm-long DFB laser with the coupling coefficient of about 33 cm^{-1}. The typical threshold current was 8 mA. The isolation resistance between the DFB laser and the modulator was more than 30 kΩ.

B. 40-Gb/s NRZ Operation

We prepared the integrated light source with a modulator length of 90 μm and 14 wells for the measurement of 40-Gb/s
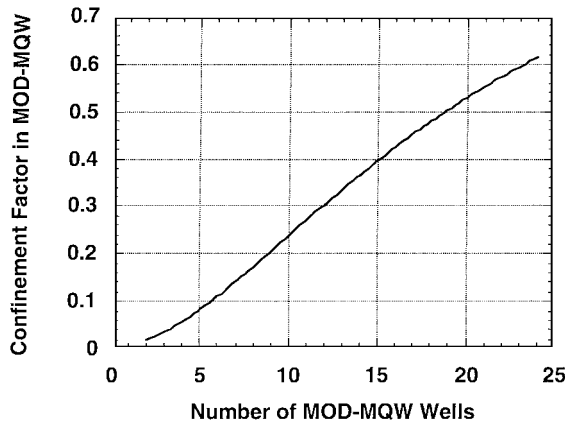
Fig. 8. Optical confinement factor of the absorption MQW layer.

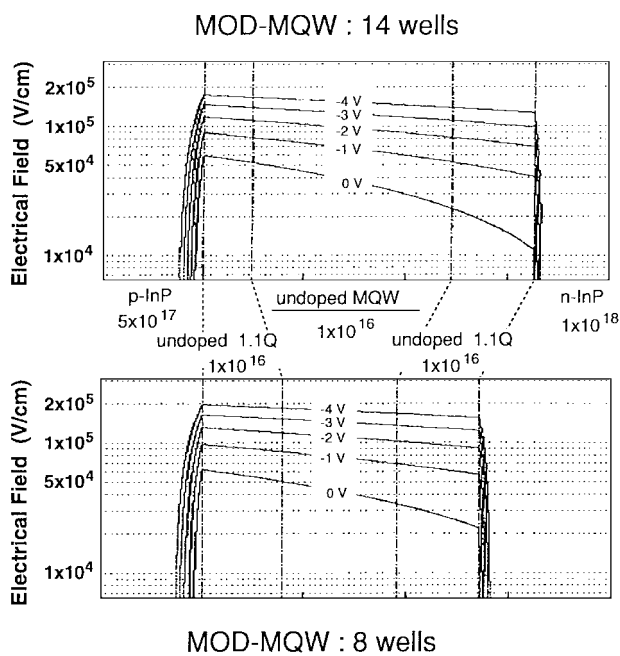Fig. 10. Photograph of the integrated light source module.

Fig. 9. The calculated electrical field distribution of the undoped layer including the MQW of the EA modulator; for 14 wells in the upper and 8 wells in the lower.

(a)

Fig. 11. The measured small-signal response (a) is for light source without polyamide and (b) is for one with polyamide.

operation. For high-speed operation at 40 Gb/s, the device should be packaged in a module to reduce the transmission loss of the electrical signal along the line. A photograph of the module is shown in Fig. 10. This compact package not only contains the integrated light source chip but also a 60-dB optical isolator, a monitor photodiode and a temperature control chip. The module is attached with an SMF. The output power from the module is 5 dBm at the injection current to the DFB laser of 80 mA and at short-circuited to the integrated modulator. The wavelength spectra exhibited a longitudinal single mode at 1.551 μm with a side-mode suppression ratio (SMSR) of 48 dB.

We measured a small-signal response prior to 40-Gb/s operation. In this measurement, the integrated modulator was biased at -1 V and the signal power was set at -10 dBm. We used two types of devices, one with no polyamide and the other with polyamide under the bonding pad to reduce the
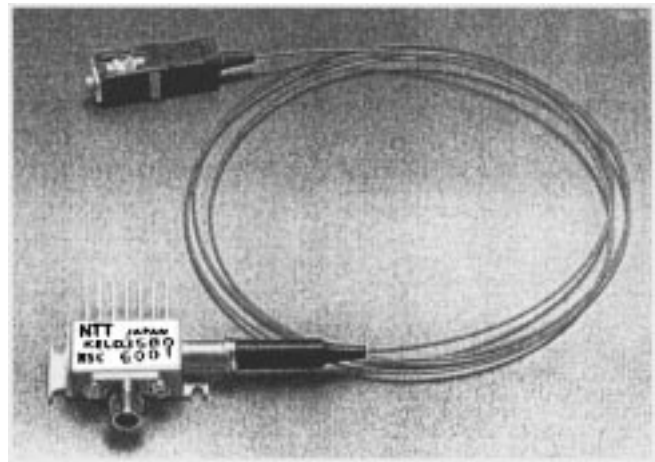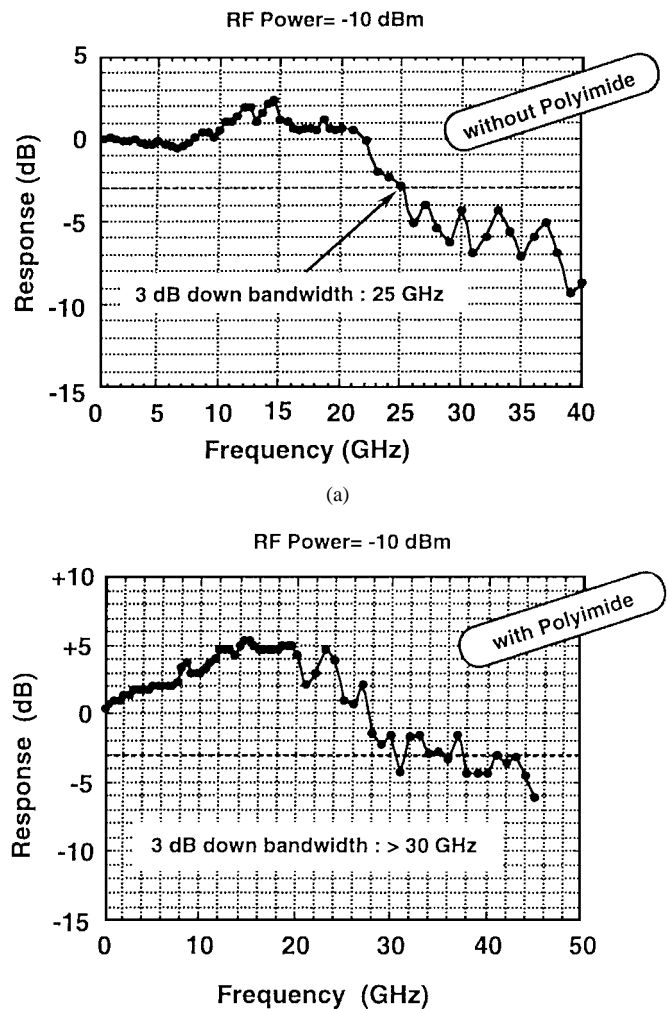
electrical capacitance. The measured 3-dB bandwidths shown in Fig. 11 were 25 GHz without polyamide on the left and over 30 GHz with polyamide on the right.

Back-to-back transmission experiments at 40 Gb/s were carried out using the setup shown in Fig. 12 [22]. It is made up
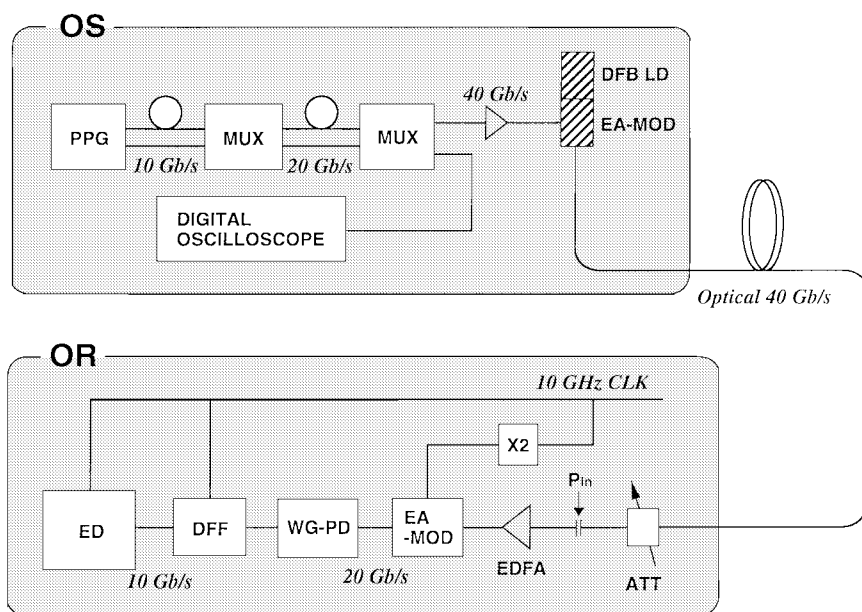
Fig. 12.   The setup for the NRZ 40-Gb/s experiment.

of an optical sender (OS) block and an optical receiver (OR) block. The high-speed light source module was used in the OS block. A 10-Gb/s nonreturn-to-zero (NRZ) electrical signal from a pulse pattern generator (PPG) was first multiplexed to 20 Gb/s and then multiplexed again up to 40 Gb/s [23]. The multiplexed 40-Gb/s driving signal was applied to the light-source module through an electrical amplifier. The peak-to-peak voltage of the driving signal was estimated to be 3 V. The waveform of the 40-Gb/s electrical signal was observed with a digtal oscilloscope. After about 5-m fiber transmission, the 40-Gb/s modulated light from the light source module was optically demultiplexed down to 20 Gb/s with an elecroabsorption modulator driven by a 20-GHz clock signal. The 20-Gb/s light was directly detected with a waveguide pin-photodiode. The input optical power at the pin-photodiode was controlled to be constant. Finally, the 20-Gb/s electrical signal was demultiplexed to 10 Gb/s in a detection circuit and led into an error detector. The receiver sensitivity was measured at a point just before the EDFA of the receiver.

The eye diagram of the 40-Gb/s modulated light from the light source module is shown in Fig. 13. The eye diagram of the driving electrical signal is also shown for reference. A clearly open eye diagram was observed, except for relative broadening of the ON state, which was due to the nonlinear attenuation of the modulator. The dynamic extinction ratio estimated from the observed eye diagram was about 10 dB. It was smaller than the static extinction ratio by about 3 dB. In the static extinction measurements, the absorbed photocurrent was generated constantly and it heated up the MQW absorption layer of the modulator. On the other hand, the heating was much less under NRZ operation. The increase in the temperature of the MQW absorption layer lengthened the exciton peak wavelength and increased absorption. In addition, the high-frequency electrical signal could not be fully applied to the integrated modulator due to reflection in the electrical signal lines and also the decreasing response at higher frequencies
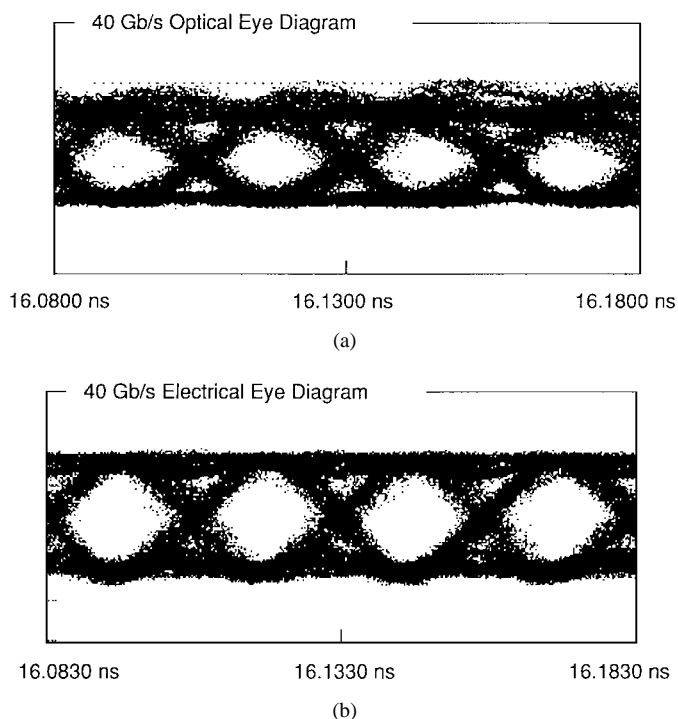

(a)

(b)

Fig. 13.   The observed eye diagram at NRZ 40-Gb/s of the modulated optical signal (upper) and the driving electrical signal (lower).

of the module. These are the reasons for the difference in the extinction ratio between static and dynamic measurements.

The BER performance of back-to-back transmission is shown in Fig. 14 for each of the four demultiplexed 10-Gb/s channels. The receiver sensitivity, measured at a bit error rate of 10^{-9}, was from -27.2 to -25.2 dBm. An error-free back-to-back transmission for each channel was confirmed down to a BER of 10^{-12}. The sensitivy of channel 3 was comparatively poor, which was mainly due to the unequal characteristics of the multiplexing electrical circuits from 20 Gb/s to 40 Gb/s.
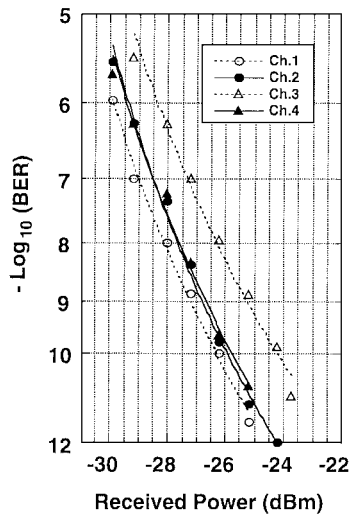
Fig. 14.   The BER performance.

Fig. 15.   The obtained optical pulse trains at a repetition rate of (a) 30 GHz and (b) 40 GHz. (I(DFB) = 100 mA, V(MOD) = −2 V.)

C. Optical Pulse Generation

When the integrated modulator was applied with a large amplitude sinusoidal voltage imposed on a reverse bias voltage, narrow optical pulse trains were obtained due to the nonlinearity of the extinction characteristics of the MQW EA modulator. This pulse generation method did not use the resonance in the integrated light source cavity. The repetition rate of the optical pulse train can be tuned very widely and very stable, because it is simply determined by the driving electrical signal. The observed optical pulse trains with repetition rates of 30 GHz and 40 GHz are shown in Fig. 15. They were observed using a streak camera system. The average pulsewidths were, respectively, 12.3 and 10.9 ps for 30 and 40 GHz. The average optical powers were −2.49 and −2.93 dBm. The extinction ratios of each pulse were 14 dB and about 9 dB. This extinction ratio reduction by increase in the repetition rate from 30 to 40 GHz was due to two reasons; the first was the reduction in the driving electrical power due to the smaller amplification at 40 GHz of the electrical amplifier, and the second was the poorer response of the integrated modulator at 40 GHz as shown in Fig. 11. The wavelength spectrum of the optical pulse at 30 GHz is shown in Fig. 16. First-to-sixth harmonics were observed with a wavelength resolution of 0.1 nm. The full width of the half maximum of the spectrum was estimated to be about 56 GHz. The time-bandwidth product was 0.69, which was much larger than that of the transform-limited optical pulse. This was caused by the frequency chirping on the integrated EA modulator due to phase modulation. From the obtained time-bandwidth product of 0.69, the α parameter of the EA modulator was estimated to be 1.2.

V. Conclusion

We developed a compact module for a high-speed integrated light source containing an electroabsorption modulator and a DFB laser for a 40-Gb/s optical transmission system. The obtained output power from the module was 5 dBm at the injection current to the DFB laser of 80 mA and at being short-circuited to the integrated modulator. High-speed operation of
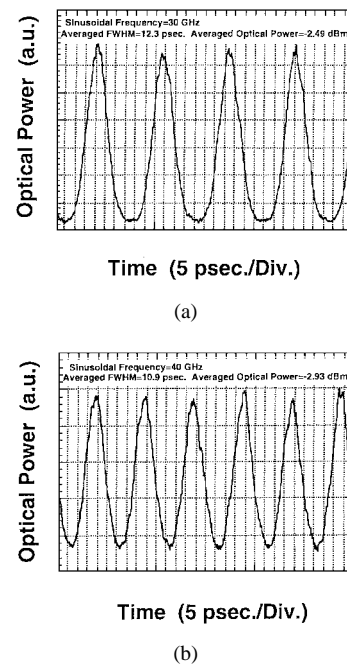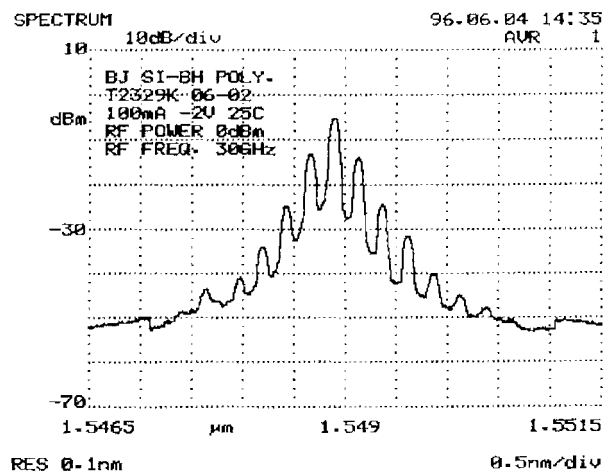

Fig. 16.   The wavelength spectrum of the optical pulse at 30 GHz.

the light source was achieved by optimizing the integrated EA modulator. A butt-joint configuration between the EA modulator and the DFB laser was employed for making it easy to perform the optimization. We obtained satisfactry small-signal response with a 3-dB bandwidth over 30 GHz and good extinction characteristics using an integrated EA modulator with 14 wells in its absorption MQW and with a length of 100 μm. We successfully performed 40-Gb/s NRZ transmission experiments. After the device was packaged into a compact module with an SMF pigtail, a multiplexed 40-Gb/s driving electrical signal was applied to the integrated modulator and a clearly-open eye diagram was observed in the output from the module. Error-free performance was confirmed and receiver sensitivity measured at a bit error rate at 10^{-9} was from −27.2 to −25.2 dBm in the back-to-back BER measurements. An optical pulse train at a repetition rate of 40 GHz was generated

with the light source module. The average pulsewidth was 10.9 ps and the average power was −2.93 dBm. We believe that the new light source module has a wide variety of applications as a light source in 40-Gb/s NRZ and RZ optical transmission systems, in a wavelength division multiplexing systems and also in microwave fiber-optic communication systems.

ACKNOWLEDGMENT

REFERENCES

[1] F. Koyama and K. Iga, "Frequency chirping in external modulators," *J. Lightwave Technol.*, vol. 6, pp. 87–93, 1988.

[2] T. Yamanaka, K. Wakita, and K. Yokoyama, "Potential chirp-free characteristics (negative chirp parameter) in electroabsorption modulator using a wide tensile-strained quantum well structure," *Appl. Phys. Lett.*, vol. 68, no. 22, pp. 3114–3116, 1996.

[3] K. Morito, R. Sahara, K. Sato, and Y. Kotaki, "Penalty-free 10 Gb/s NRZ transmission over 100 km of standard fiber at 1.55 μm with a blue-chirp modulator integrated DFB laser," *IEEE Photon. Technol. Lett.*, vol. 8, pp. 431–433, 1996.

[4] T. Ido, S. Tanaka, M. Suzuki, and H. Inoue, "An ultra-high-speed (50 GHz) MQW electro-absorption modulator with waveguides for 40 Gbit/s optical modulation," in *Tech. Dig. 10th Int. Conf. Integrated Optics and Optical Fiber Communication (IOOC'95)*, 1995, pp. 1–2, paper PD1-1.

[5] O. Mitomi, I. Kotaka, K. Wakita, S. Nojima, K. Kawano, Y. Kawamura, and H. Asai, "40-GHz bandwidth InGaAs/InAlAs multiple quantum well optical intensity modulator," *Appl. Opt.*, vol. 31, pp. 2030–2035, 1992.

[6] K. Satzke, D. Baums, U. Cebulla, H. Haisch, D. Kaiser, E. Lach, E. Kuhn, J. Weber, R. Weinmann, P. Wiedemann, and E. Zielinski, "Ultrahigh-bandwidth (42 GHz) polarization-independent ridge waveguide electroabsorption modulator based on tensile strained InGaAsP MQW," *Electron. Lett.*, vol. 31, pp. 2030–2032, 1995.

[7] F. Devaux, S. Chelles, J. C. Harmand, N. Bouadma, F. Huet, M. Carre, and M. Foucher, "Polarization independent InGaAs/InAlAs strained MQW electroabsorption modulator with 42 GHz bandwidth," in *Tech. Dig. 10th Int. Conf. Integrated Optics and Optical Fiber Communication (IOOC'95)*, 1995, vol. 4, pp. 56–57.

[8] F. Devaux, F. Dorgeuille, A. Ougazzaden, F. Huet, M. Carre, A. Carenco, M. Henry, Y. Sorel, J. F. Kerdiles, and E. Jeanney, "20 Gbit/s operation of a high-efficiecy InGaAsP/InGaAsP MQW electroabsorption modulator with 1.2-V drive voltage," *IEEE Photon. Technol. Lett.*, vol. 5, pp. 1288–1290, 1993.

[9] T. Ido, H. Sano, D. A. Moss, S. Tanaka, and A. Takai, "Strained InGaAs/InAlAs MQW electro-absorption modulators with large bandwidth and low driving voltage," *IEEE Photon. Technol. Lett.*, vol. 6, pp. 1207–1209, 1994.

[10] A. Ramdane, D. Delprat, F. Devaux, D. Mathoorasing, A. Ougazzaden, N. Souli, F. Delorme, and J. Landreau, "Multiple quantum well distributed feedback laser-electroabsorption modulator light source with 36 GHz bandwidth," in *Tech. Dig. Pacific Rim Conf. Lasers and Electro-Optics*, 1995, p. 222.

[11] K. Wakita, K. Sato, I. Kotaka, M. Yamamoto, and T. Kataoka, "20 Gbit/s, 1.55 μm strained-InGaAsP MQW modulator integrated DFB laser module," *Electron. Lett.*, vol. 30, no. 4, pp. 302–303, 1994.

[12] A. Ramdane, D. Delprat, A. Ougazzaden, Y. Sorel, J. F. Kerdiles, M. Henry, and C. Thebault, "High performance strained layer integrated laser-modulator for 20 Gbit/s transmission," in *Proc. 22th Eur. Conf. Optical Communication (ECOC'96)*, 1996, pp. 3.191–3.194.

[13] E. Yamada, K. Wakita, and M. Nakazawa, "30 GHz pulse train generation from a multiquantum well electroabsorption intensity modulator," *Electron. Lett.*, vol. 29, no. 10, pp. 845–846, 1993.

[14] H. Soda, K. Nakai, and H. Ishikawa, "Frequency response of an optical intensity modulator monolithically integrated with a DFB laser," in *Proc. 14th Eur. Conf. Optical Communication (ECOC'88)*, 1988, pp. 227–230.

[15] K. Komatsu, T. Kato, M. Yamaguchi, T. Sasaki, S. Takano, H. Shimizu, N. Watanabe, and M. Kitamura, "High-performance modulator/integrated light sources grown by an in-plane band-gap

[16] energy-control technique," in *Tech. Dig. Optical Fiber Communication (OFC'94)*, 1994, vol. 4, pp. 8–9.

[16] M. Aoki and H. Sano, "High-performance modulator/integrated light sources grown by an in-plane band-gap energy-control technique," in *Tech. Dig. Optical Fiber Communication (OFC'95)*, 1995, vol. 8, pp. 25–26.

[17] J. E. Johnson, P. A. Morton, T. Nguyen, O. Mizuhara, S. N. G. Chu, G. Nykolak, T. Tanbun-Ek, W. T. Tsang, T. R. Fullowan, P. F. Sciortino, A. M. Sergent, K. W. Wecht, and R. D. Yadvish, "10-Gbit/s transmission using an integrated electroabsorption-modulator/DFB laser grown by elective-area epitaxy," in *Tech. Dig. Optical Fiber Communication (OFC'95)*, 1995, vol. 8, pp. 21–23.

[18] H. Haisch, W. Baumert, C. Hache, E. Kühn, M. Klenk, K. Satzke, M. Schilling, J. Weber, and E. Zielinski, "10 Gbit/s standard fiber TDM transmission at 1.55 μm with low chirp monolithically integrated MQW electroabsorption modulator/DFB-laser realized by selective area MOVPE," in *Proc. 20th Eur. Conf. Optical Communication (ECOC'94)*, 1994, pp. 801–804.

[19] J. A. Fells, M. A. Gibbon, G. H. B. Thompson, I. H. White, R. V. Penty, A. P. Wright, R. A. Sauders, C. J. Armistead, and E. M. Kimber, "Improving the system performance of integrated MQW laser modulators with negative chirp," in *Tech. Dig. Optical Fiber Communication (OFC'95)*, 1995, vol. 8, pp. 23–24.

[20] S. Matsumoto, M. Fukuda, K. Sato, Y. Itaya, and M. Yamamoto, "Highly reliable 1.55 μm GaInAsP laser diodes buried with semi-insulating iron-doped InP," *Electron. Lett.*, vol. 30, no. 16, pp. 1305–1306, 1994.

[21] T. Yamanaka, K. Wakita, and K. Yokoyama, "Field-induced broadening of optical absorption in InP-based quantum wells with strong and weak quantum confinement," *Appl. Phys. Lett.*, vol. 65, no. 12, pp. 1540–1542, 1994.

[22] A. Sano, T. Kataoka, H. Tsuda, A. Hirano, K. Murata, H. Kawakami, Y. Tada, K. Hagimoto, K. Sato, K. Wakita, K. Kato, and Y. Miyamoto, "Field experiments on 40 Gbit/s repeaterless transmission over 198 km dispersion-managed submarine cable using a monolithic mode-locked laser diode," *Electron. Lett.*, vol. 32, no. 13, pp. 1218–1220, 1996.

[23] T. Otsuji, M. Yoneyama, Y. Imai, S. Yamaguchi, T. Enoki, Y. Umeda, and E. Sano, "46 Gbit/s multiplexer and 40 Gbit/s demultiplexer IC modules using InAlAs/InGaAs/InP HEMT's," *Electron. Lett.*, vol. 32, no. 7, pp. 685–686, 1996.

Hiroaki Takeuchi, photograph and biography not available at the time of publication.

Ken Tsuzuki, photograph and biography not available at the time of publication.

Kenji Sato (M'95), for photograph and biography, see this issue, p. 255.

Mitsuo Yamamoto, for a biography, see this issue, p. 255.

Yoshio Itaya, photograph and biography not available at the time of publication.

Akihide Sano, photograph and biography not available at the time of publication.

Mikio Yoneyama, photograph and biography not available at the time of publication.

Taiichi Otsuji, photograph and biography not available at the time of publication.